Krystian SZOPA
Marek IWANIEC
Joanna IWANIEC

IDENTIFICATION OF TECHNICAL CONDITION OF THE OVERHEAD POWER LINE SUPPORTING STRUCTURE

IDENTYFIKACJA STANU TECHNICZNEGO KONSTRUKCJI WSPORCZEJ NAPOWIETRZNEJ LINII ELEKTROENERGETYCZNEJ*

Technical diagnostics of the overhead power line supporting structures is very important from the point of view of reliability and the national energy security. The paper presents a method of identification of technical condition of power line supporting structures. The technique is based on testing the correlation between the change of stress in the system and the change of modal parameters caused by damage. Presented approach is comprehensive and accounts for a number of problems related to the diagnostics of large-size objects of complex geometry. The basic advantage of the developed identification algorithm of the overhead power line supporting structures technical condition is low sensitivity to measurement errors, which is very important in the context of exploitational diagnostics.

Keywords: *modal analysis, technical diagnostics, finite element method.*

Diagnostyka techniczna konstrukcji wsporczych napowietrznych linii elektroenergetycznych jest zagadnieniem niezwykle istotnym z punktu widzenia niezawodności i bezpieczeństwa energetycznego kraju. W artykule przedstawiono metodę identyfikacji stanu technicznego kratownicowych konstrukcji wsporczych. Technika jest oparta na badaniu korelacji pomiędzy zmianą stanu naprężenia w układzie, a zmianą parametrów modalnych, spowodowanych uszkodzeniem. Zaprezentowane podejście jest kompleksowe i uwzględnia szereg problemów związanych z diagnostyką obiektów wielkogabarytowych o złożonej geometrii. Podstawową zaletą opracowanego algorytmu identyfikacji stanu technicznego konstrukcji wsporczych jest niska wrażliwość na błędy pomiarowe, co jest niezwykle istotne w kontekście diagnostyki eksploatacyjnej.

Słowa kluczowe: *analiza modalna, diagnostyka techniczna, metoda elementów skończonych.*

1. Introduction

Electric power is a basic energy medium, necessary for transport, industry, institutions, businesses and households. A reliable power distribution system is of key importance for the national energy security. Mechanical failure of a power line results in a blackout, which leaves thousands of people deprived of electricity and causes transport and industry stoppage. For the operator it entails not only the repair costs, but also penalties and compensations. In the recent years the largest power failures in Poland took place in Zachodniopomorskie Province in April of 2008 [2, 21], in Małopolskie Province in January of 2010 [6, 12] and also in Świebodzice (2012) on the Tarnów-Olszyny line [25]. In almost each case of catastrophe the expertises have proven that the failure resulted directly from poor weather conditions, and indirectly from negligence related to the infrastructure maintenance. The results presented in [4] confirm that in case of an overhead power line it is important to monitor not only the weather loads but also the line technical condition. In addition, according to the information given by Energy Regulatory Office in 2017, 54% of overhead power lines owned by the TSO (**T**ransmission **S**ystem **O**perator) and 36% lines owned by DSOs (**D**istribution **S**ystem **O**perators) are more than 40 years old, and in the 1970s the lines were designed for 65% of currently permissible loads [21]. Such extensive infrastructure requires continuous inspections, modernization and renovation in order to ensure security and reliability. Identification of supporting

structures technical condition allows to focus these activities on the proper areas.

Most methods of non-destructive testing (NDT) find applications in detection of local damages, in small elements. In case of large and complex structures such methods are labour-consuming and often uneconomic. Therefore, vibroacoustic methods are an important group of the NDT. The essence of vibroacoustic methods consists in testing the changes in the object dynamic properties that occur as a result of local change of stiffness caused by damage. Modal parameters can describe a system in a global or local way. In case of damage detection in supporting structures of overhead power lines it is also important that the NDT methods can be used in the structural health monitoring system (SHM), which in recent years has played an increasingly important role in the diagnostics of engineering structures. The SHM involves a periodic reading of information from a network of sensors placed on the monitored object and then interpretation of such data in relation to the structure technical condition. Additional storage of information over such a long period of time allows for making statistics and foreseeing the structure life [5]. The essence of the system is a remote observation of an object based on data sent to the central unit [11].

The detailed analytical and critical research indicates that verification of the vibroacoustic diagnostic methods is usually limited to simple structures (single support beams, plates, simple frames) [8, 15, 19] or only to simulation tests in which the number of

---

simplifications is introduced. In practice such techniques, often with a complex mathematical apparatus, are difficult to apply to objects of complex geometry. Even if some methods are used for such objects, simplifications are made in terms of limiting the damage search area and neglecting the impact of damage outside this area on the structure dynamic characteristics [17].

The basic problem in application of vibroacoustic methods to damage detection in objects of complicated geometry (particularly in overstiffed objects such as truss supporting structures) is low sensitivity of modal parameters to single damage, which in turn results in ill-conditioning of the inverse models. Even small measurement, estimation and modelling errors have a strong impact on the results, leading to ambiguity or a total loss of the solution convergence. Other obstacles in identification of technical condition of large-size objects include nonlinear relationship between modal parameters and the stiffness of individual elements, identification of natural frequencies between the damaged and undamaged structure without the measurement of mode shapes, identification of the numerical model parameters based on the *a priori* knowledge, limited number of measurement points and the amount of obtained information, changes in boundary conditions (e.g. ambient temperature). These conclusions arise from both the literature review [10] and many studies conducted by the authors of this paper [13, 14, 23, 24]. The state of art analysis indicates that the best solution for the diagnostics of supporting structures of overhead power lines can be the methods based on the analysis of the system mode shapes, assuming a limited number of measurement points.

2. Research object and identification of its technical condition

A simplified physical model of the overhead power line supporting structure was designed and made in order to conduct the studies (Fig. 1). The tower model was made of steel, and is a spatial, bolted truss structure. The tower height is 2.65 m, which is approximately 1/10 of the height of such objects used in power engineering. The main legs (kerbs) were made of L25 × 25 × 3 angles and each leg consists of two bars connected to each other 1.5 m above the base. The base frame made of identical sections is used to fasten the structure to the foundation. The cross-arms are made of L20 × 20 × 2 angles. Secondary elements placed horizontally and diagonals are 10 × 5 mm bars (Table 1). Usage of elements of square cross sections instead of elements of circular cross sections makes it possible to mount the elements in nodes with the application of bolting connections. Carried out research aimed at analysis of dynamic properties of a truss system of complex geometry and identification of its technical condition.
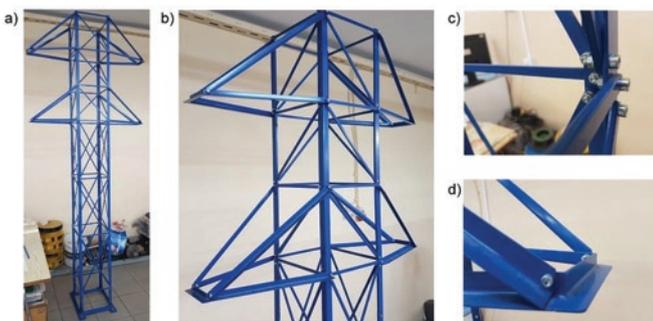
Table 1. Cross sections and materials of supporting structure

	Legs	Secondary elements	Cross-arms
Cross section shape [mm]	L 25×25×3	Flat 10×5	L 20×20×2
Cross section [m²]	$1.42 \cdot 10^{-4}$	$50 \cdot 10^{-6}$	$73 \cdot 10^{-6}$
Geometrical moment of inertia [I_z] [m⁴]	$0.8 \cdot 10^{-8}$	$1.04 \cdot 10^{-10}$	$0.28 \cdot 10^{-8}$
Geometrical moment of inertia [I_y] [m⁴]	$0.8 \cdot 10^{-8}$	$4.17 \cdot 10^{-10}$	$0.28 \cdot 10^{-8}$
Young's modulus [Pa]	$2.05 \cdot 10^{11}$	$2.05 \cdot 10^{11}$	$2.05 \cdot 10^{11}$
Kirchhoff's modulus [Pa]	$8 \cdot 10^{10}$	$8 \cdot 10^{10}$	$8 \cdot 10^{10}$
Density [kg/m³]	7870	7870	7870

The next stage of the research consisted in development of the algorithm for identification of the supporting structure technical condition (Fig. 2). The proposed method involves comparison of modal parameters (taking into account mode shapes) of the damaged and undamaged structure. The adjusted numerical model of the object is used to determine the measured (main) degrees of freedom and for the purposes of static strength analysis. In the course of the research damage was introduced to the structure and, based on the regression analysis, it was possible to develop the linear characteristics that accounts for relationship between maximum stress and the averaged value of MAC (**M**odal **A**ssurance **C**riterion) as a result of changes in the stiffness. For determined characteristic the $MAC_{av,g}$ limit values are determined, which define intervals of the supporting structure technical conditions. Damage occurring during the operation is classified as one of the possible technical conditions based on the $MAC_{av,d}$ value that compares the mode shapes of the system in the present (investigated) condition to the mode shapes of the undamaged structure.
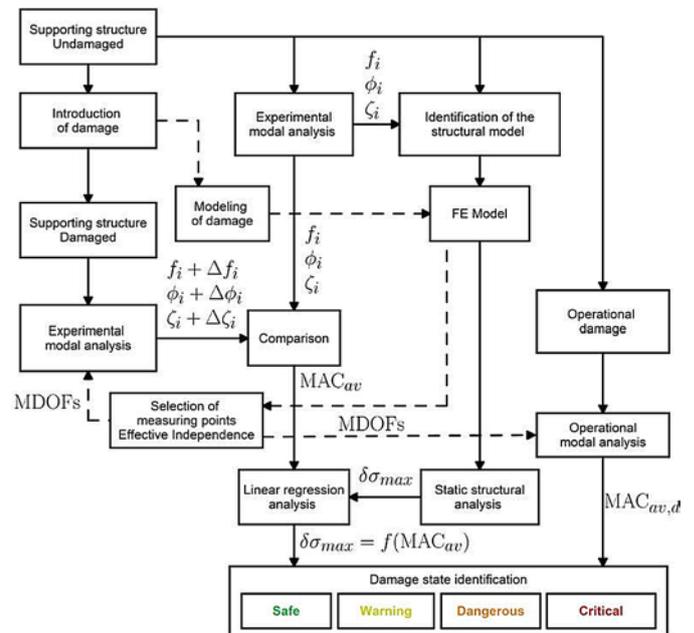
Fig. 2. Algorithm for identification of the supporting structure technical condition

Fig. 1. Supporting structure physical model

3. Experimental modal analysis of supporting structure and identification of numerical model parameters

The next stage involved an experimental modal analysis of the object, determining an ordered set of natural frequencies, modal damping ratios and mode shapes. Fig. 3b shows 36 points in which the modal displacement was measured in directions *X* and *Y*. This means that mode shapes were determined based on 72 measured degrees of freedom. Two vibration sensors (uniaxial piezometric accelerometers for each direction *X* and *Y*) were placed in point 26.
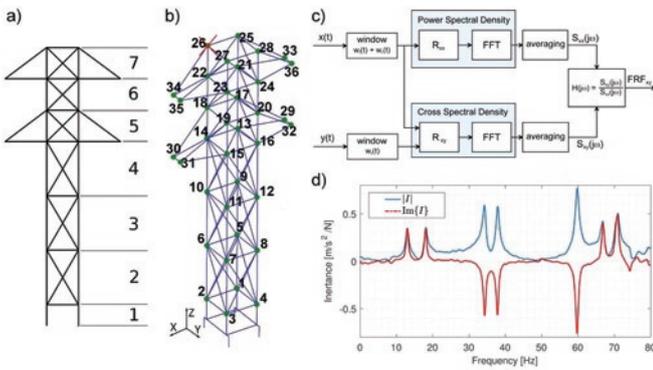
Fig. 3. Experimental modal analysis (a) division of geometric model into segments, (b) measurement points (measurements in directions X and Y were taken in each point), (c) scheme of processing the excitation and response time signals to the transfer function form, (d) system inertance for excitation in point 12X and response in point 26X

As the result of measurements time series of excitation and response signals were obtained (Fig. 5). Fast Fourier Transform (FFT) was applied to transform the signals from time to frequency domain. Since in lightly damped systems the response signal usually does not fade at the end of the signal recording time, the following exponential window was used in order to minimize the spectral leakages:

$$w_r = e^{-\beta t}, \qquad \beta = \frac{1}{\tau} \quad , \qquad (1)$$

and a window with the Tikhonov filter function was used for the input signal:

$$w_f = 1 - \frac{t^n}{t^n + \alpha^n} \quad . \qquad (2)$$

Estimator H_1 (Fig. 3c), expressed by relationship [9], was used to determine the system transfer functions:

$$H_{xy}(j\omega) = \frac{S_{xy}(j\omega)}{S_{xx}(j\omega)}, \qquad (3)$$

where S_{xx} is the input signal spectral power density, a S_{xy} is the input and output cross-spectral density. Fig. 3d presents an example of frequency domain transfer function of the system in the form of inertance between points 12 and 26 in direction *X*.

Estimation of modal parameters was performed using the RFP (**R**ational **F**raction **P**olynomial) method [22], which involves fitting the

characteristics in the frequency domain expressed in the form of a rational function. Determined modal parameters of the considered supporting structure are given in Table 2. The values of undamped natural frequencies were calculated using the corrected damping coefficients (due to the use of exponential window). Note an insignificant impact of the damping coefficient on the difference between damped and undamped natural frequencies of truss supporting structures. The maximum relative change of the first frequency amounted to 0.05%. Due to the limited conditions of the experiment, 6 mode shapes were fully determined.

Numerical model was built as a spatial frame structure (Fig. 4a). As a result of discretization, the numerical model connects 112 beam elements in 40 nodes, each element has 6 degrees of freedom. An additional degree of freedom for vertical translation at restraint, for each anchor, gives a model of 244 degrees of freedom. As the slenderness ratio of elements is relatively high, the elements conforming to the Euler-Bernoulli beam theory were used (Fig. 4b).

An additional finite element was introduced to connect two nodes and allow defining the stiffness coefficients between respective degrees of freedom of these nodes (Fig. 4e). This element was used to model the bolted joint between secondary elements and the tower legs (Fig. 4d). The model includes displacements of the fastening points between the structure and the base in global direction *Z*. The boundary conditions, according to Fig. 4c, are as follows:

$$u(L,t) = \theta(L,t) = v(L,t) = \frac{\partial v}{\partial x}(L,t) = \frac{\partial w}{\partial x}(L,t) = 0,$$

$$\frac{\partial}{\partial x}\left(EI\frac{\partial^2 w}{\partial x^2}(L,t)\right) = k_f w(L,t), \qquad (4)$$

where $u(x,t)$ is the function of points displacements along axis *x*, Δf_i is the function describing rotation of the cross sections, $v(x,t)$ and $w(x,t)$ are deflection functions in planes *xy* and *xz*, and k_f denotes stiffness of a single anchor bolt.

Numerical model of supporting structure was compared with the experimental model (Table 3). For five mode shapes the difference in obtained natural frequencies was small and did not exceed 3%. Only for the fifth natural frequency the difference is greater and equals 10%. Estimated mode shapes are shown in Fig. 5. The mode shapes were compared using the MAC criterion [1]

$$MAC_i = \frac{\left|\psi_{i,exp}^H \cdot \psi_{i,num}\right|^2}{\left(\psi_{i,exp}^H \cdot \psi_{i,exp}\right)\cdot\left(\psi_{i,num}^H \cdot \psi_{i,num}\right)} , \qquad (5)$$

Table 2. *Structure modal parameters determined with the application of experimental modal analysis*

Mode shape	$\hat{\sigma}_i$	σ_i	ω_i	f_i	ω_t^i	f_t^i	ζ_i
	[rad/s]	[rad/s]	[rad/s]	[Hz]	[rad/s]	[Hz]	[%]
1	−2.51	−1.40	81.66	13.00	81.62	12.99	1.72
2	−2.76	−1.48	113.15	18.01	113.12	18.00	1.31
3	−2.78	−1.49	215.79	34.34	215.77	34.34	0.69
4	−2.51	−1.40	237.97	37.88	237.96	37.87	0.59
5	−3.02	−1.58	375.45	59.76	375.44	59.75	0.42
6	−2.55	−1.42	442.48	70.42	442.46	70.42	0.32

Designations in the Table: $\hat{\sigma}_i$ – damping coefficient determined for the characteristics damped with exponential window, σ_i – adjusted damping coefficient, ω_i, f_i – angular frequency and frequency of undamped free vibration, ω_t^i, f_t^i – angular frequency and frequency of damped free vibration, ζ_i – modal damping ratio (adjusted)

Table 3.   *Comparison of natural frequencies and mode shapes of the experimental and numerical models*

Mode shape	f_i^{exp}	f_i^{num}	Δf_i [Hz]	δf_i [%]	MAC_i
1	13.00	13.22	0.22	1.69	0.95
2	18.01	18.31	0.30	1.67	0.97
3	34.34	34.13	−0.21	−0.61	0.86
4	37.88	38.99	1.11	2.93	0.85
5	59.76	65.76	6.00	10.04	0.88
6	70.42	70.03	−0.39	−0.55	0.72

Fig. 4.   *Finite element model (a) supporting structure, (b) finite element in local system, (c) boundary condition for anchor joint, (d) bolted joints of physical model bars, (e) elastic joint model for bolted joint*

complicated shape of this mode (greater number of vibration nodes) and also from an additional connection of the top and bottom parts of the tower stem, which was not accounted for in then numerical model. The increased stiffness of the middle belt part affects the vibration node location with respect to the leg length.

4. Preliminary damage impact analysis and measuring mesh

Two damage cases were analysed. Damage U_1 was introduced by removing members denoted as 30, 59, 60 from the supporting structure (Fig. 9). All the elements are neighbouring with each other and form X-braced panel of one of the structure walls in its lower part. Damage U_2 was introduced by removing elements 34, 57, 59, 68 from the supporting structure. These elements are located in successive tower sections, and none of them forms X-bracing with another one.

An experimental modal analysis was performed for both cases. Table 4 includes the analysis results and comparison with the dynamic response of undamaged model Z_1. Although more elements were damaged in case U_2 than in case U_1, the changes in modal parameters were definitely greater in case U_1. This confirms a redundant character of the studied structure. Damages of single secondary elements in various tower sections and walls does not have a significant impact on the system response and the structure maintains high stiffness. However, a damage of bracing members in the same section and wall significantly affects the object dynamic behaviour.

For the purposes of more detailed analysis more damage cases must be considered. Unfortunately, in this case, estimation of the considered system mode shapes requires determination of modal displacement for 72 degrees of freedom. Measurement of such a large number of transfer functions is time-consuming. In addition, it should be em-

which defines the correlation degree between the experimental model modal vectors $\psi_{i,exp}$ and the numerical model modal vectors $\psi_{i,num}$. The first and the second mode shapes are bending modes similar to mode shapes of a cantilever beam, while the MAC value for these modes is very high. For mode shapes $3 \div 5$, the obtained MAC values are not lower than 0.85, which is a good result for such structures. For the last, 6th mode shape the MAC value is lower than for the other mode shapes, which can result from the

Table 4.   *Comparison of natural frequencies for damage cases U_1 and U_2 to natural frequencies of undamaged structure Z_1*

Mode shape	Z_1	U_1				U_2			
	f_i [Hz]	f_i [Hz]	Δf_i [Hz]	δf_i [%]	MAC_i	f_i [Hz]	f_i [Hz]	Δf_i [%]	δf_i [Hz]
1	13.00	11.15	−1.85	−14.25	0.75	12.98	−0.02	−0.13	0.99
2	18.01	15.21	−2.80	−15.56	0.62	17.63	−0.38	−2.13	0.99
3	34.34	23.94	−10.41	−30.3	0.61	31.56	−2.78	−8.1	0.93
4	37.88	37.40	−0.48	−1.26	0.89	37.85	−0.03	−0.07	0.97
5	59.76	59.70	−0.06	−0.09	0.77	59.74	−0.02	−0.03	0.95
6	70.42	66.82	−3.60	−5.11	0.72	70.14	−0.28	−0.4	0.92

Fig. 5   *Comparison of mode shapes obtained in the course of the experimental and numerical investigation: (a) 1st, (b) 2nd, (c) 3rd, (d) 4th, (e) 5th, (f) 6th mode shape*

phasized that the measurement of the industrial supporting structure displacements in directions X and Y in all the nodes is not possible. Therefore, the number of measuring points must be limited and the sensors must be placed in such a manner as to obtain the maximum amount of information.

The measuring mesh for the studied supporting structure model was defined using the EI (**E**ffective **I**ndependence) method [16], which is simple and gives good results. This technique was used in [26] for sensors placement on a plate with the application of genetic algorithms. The EI method allows for selecting a set of measuring points for which the analysed modal displacements are most linearly independent from each other, simultaneously containing enough information about the dynamic behaviour of the object. The method involves determination of a

vector that includes the elements lying on the diagonal of a matrix determined as follows:

$$EI = diag\left[\psi \left(\psi^T \psi \right)^{-1} \psi^T \right] \qquad (6)$$

where ψ is a matrix of considered mode shapes and degrees of freedom. Each element of vector EI corresponds to a specific degree of freedom (potential measuring point) and is a component necessary to determine the rank of the matrix, which can be of the full rank only when the mode shapes are linearly independent. In order to determine the measuring points, the modal matrix must be limited to the measured mode shapes. In the subsequent iterations the degrees of freedom that have the least contribution to the linear independence between mode shapes must be rejected. Each time a new EI vector is calculated and the iterations are repeated until the dimension corresponding to the required number of measuring points N_m is reached.

Difference between the mean MAC value for limited number of sensors and the mean MAC value for the measurement of modal displacements at all 72 degrees of freedom was assumed as the sensors placement criterion:

$$\Delta \text{MAC}_{av} = \text{MAC}_{av}^{N_m} - \text{MAC}_{av} \qquad (7)$$

while:

$$\text{MAC}_{av}^{N_m} = \sum_{i=1}^{6} \frac{\text{MAC}_i^{N_m}}{6} \qquad (8)$$

and:

$$\text{MAC}_{av} = \sum_{i=1}^{6} \frac{\text{MAC}_i}{6} \qquad (9)$$

where MAC_i and $\text{MAC}_i^{N_m}$ were calculated between the modal vectors of undamaged and damaged structure, for respectively all 72 measured degrees of freedom and limited number of N_m degrees of freedom.
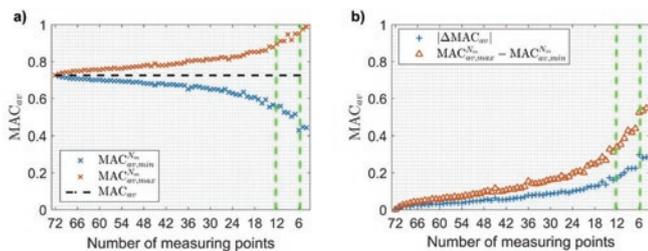
Fig. 6. Comparison of mode shapes for cases U_1 and Z_1 for extremely unfavourable placement of measuring points (a) maximum and minimum $\text{MAC}_{av}^{N_m}$ values, (b) ΔMAC_{av} value (7) and range of $\text{MAC}_{av}^{N_m}$ values

Fig. 6 presents the results for an extremely unfavourable placement of measuring points. Mode shapes for conditions U_1 and Z_1 were compared using the MAC criterion. 10000 random measuring meshes were generated for each number of sensors, and two extreme cases were chosen for the maximum and minimum MAC value (Fig. 6a). Obtained results proved that decrease in the number of measured degrees of freedom results in the increase in the range of MAC values. This means that for the same supporting structure technical condition the MAC_{av} value may differ depending on the selection of measuring
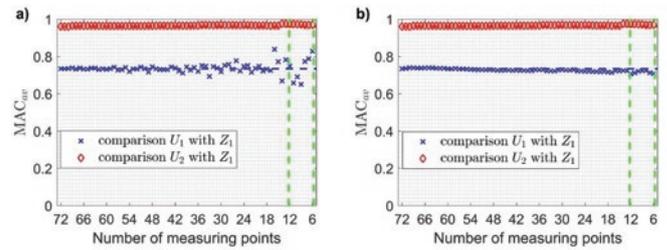
Fig. 7. $\text{MAC}_{av}^{N_m}$ values comparing the mode shapes for states U_1 and U_2 to Z_1 for different types of measuring points placement: (a) random, (b) according to the Effective Independence algorithm

points. For example, for 9 measuring points the measurement with a given measuring mesh will give the result equal to 0.95, whereas for a different sensors placement the result will be 0.52. The value range is 0.43 and the MAC_{av} value for the full number of sensors lies approximately in the middle and equals 0.73. This totally changes the structure classification in terms of technical condition. It is worth mentioning that the number of measuring points that we are interested in is between 6 and 12, where the range is the greatest (Fig. 6b). For this reason, the selection of measured degrees of freedom is so important.

The mesh of measuring points was determined according to the EI algorithm based on mode shapes obtained for the numerical model for each number of sensors from 6 to 71. Calculated $\text{MAC}_{av}^{N_m}$ values are presented in Fig. 7b. The distance of these values from MAC_{av} determined for the full number of sensors is maximum 0.02 for 12 measuring points while comparing U_1 and Z_1, which is a very small difference considering a significant benefit of a reduced number of measurements. The ΔMAC_{av} values determined for conditions U_2 and Z_1 are even smaller. For comparison, Fig. 7a shows a case for random placement of sensors. The ΔMAC_{av} value equals -0.09, while the range amounts to almost 0.18.

Fig. 8 presents 3 examples of sensors placement according to the EI algorithm. Selected measuring points are written in vectors MP_{N_m}. Designation of measuring points conforms to Fig. 5:

$$MP_{12} = \left[5X, 7X, 8X, 26X, 28X, 5Y, 25Y, 26Y, 27Y, 28Y, 33Y, 34Y \right]$$

$$MP_9 = \left[5X, 7X, 8X, 26X, 28X, 26Y, 28Y, 33Y, 34Y \right]$$

$$MP_6 = \left[7X, 8X, 26X, 26Y, 28Y, 33Y \right]$$

Since the EI algorithm is iterative, each mesh with a smaller number of measuring points is a subset of previous meshes.
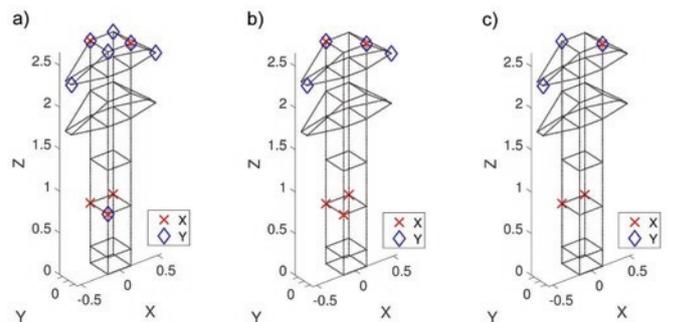
Fig. 8. Mesh of measuring points determined with the application of the Effective Independence algorithm for (a) 12, (b) 9 and (c) 6 measuring points

Most of the measuring points are located at the top of the transmission tower stem, which is influenced mainly by the 1st and the 2nd mode shapes; the largest modal displacements are observed there for these modes. The measuring points located on the cross-arms result mainly from the 3rd mode shape, which is a torsional mode. The measurement of modal displacements in the middle part of the tower stem, between section 2 and 4, allows for observing mainly the 5th but also 4th and 6th mode shapes (Fig. 5).

5. Identification of structure technical condition

Seven cases of supporting structure damages were analysed and, as a result of modal analysis, the sets of natural frequencies, modal damping ratios and mode shapes were determined. Six mode shapes were taken into account for each case. For the first and the second damage condition, the mode shapes include modal displacements in 72 degrees of freedom ($1 \div 36$ X, Y, acc. to Fig. 3b), whereas for cases $3 \div 7$ they account for 12 degrees of freedom determined in accordance with the EI algorithm (6) (Fig. 8a). Since the number of determined modal displacements is large for all damage cases and all the mode shapes, this parameter was included in the MAC criterion by comparing the mode shapes of damaged and undamaged structures. All the results are given in Table 4.

Identified supporting structure numerical model was subjected to forces that simulate loading with wires at difficult weather conditions (Fig. 9b). The load values were determined analogously as in the case described in [4], however taking into account dimensions of the laboratory model. The analysed case included an asymmetric icing of the wires along the overhead line, with an additional perpendicular force caused by the wind. Each of two separately analysed conditions results in structure bending in two planes perpendicular to each other. Combining the discussed cases into one loading condition makes it possible to take into account the impact of damaged elements in each structure wall on the change of maximum stress in the system. The calculated load values are as follows:

$$V = 114 \text{ N}, \quad H_1 = 583 \text{ N}, \quad H_2 = 852 \text{ N}, \quad P = 78 \text{ N},$$

according to the designations shown in Fig. 9b. The same load condition was used for each case, and the maximum stress that occurred in the structure was determined and compared with stress in the undamaged structure.

In case of damage U_1, the removed elements are X-bracing of section 2 of one of the walls (Fig. 9a). As the truss is located near the legs restraint to the base, where the highest stress for the set load occurs, such damage has a huge impact on the stress in the structure and is close to the yield stress of the S235JR material. There is a significant impact of the damage on the modal parameters for the first three natural frequencies. However, it must be emphasized that the change of modal damping ratio ζ_1 results mainly from the frequency change, whereas the damping coefficient value relative to σ_1 did not change significantly. The MAC values reach an average of 0.72, indicating a noticeable change in the mode shape with respect to the undamaged condition. In case of damage condition U_3 only one lower section diagonal was removed. The change in modal parameters is insignificant

Table 5. *Comparison of modal parameters determined for considered damage cases to parameters of undamaged structure*

Condition	Z_1	U_1	U_2	U_3	U_4	U_5	U_6	U_7
Damaged elements acc. to Fig. 9a	--	30	34	30	34	38	38	30
	--	59	57	60	67	75	75	59
	--	60	59	--	68	76	76	60
	--	--	68	--	--	--	39	31
	--	--	--	--	--	--	77	61
	--	--	--	--	--	--	78	62
f_1 [Hz]	13.00	11.15	12.98	12.95	12.32	12.39	12.26	11.13
f_2 [Hz]	18.01	15.21	17.63	17.86	16.35	16.27	13.93	10.34
f_3 [Hz]	34.34	23.94	31.56	32.07	26.77	26.06	23.65	22.24
f_4 [Hz]	37.88	37.40	37.85	37.64	37.44	37.43	37.44	34.40
f_5 [Hz]	59.76	55.40	59.74	56.46	59.67	58.71	53.65	54.55
f_6 [Hz]	70.42	67.65	70.14	68.91	69.41	70.11	69.47	67.23
ζ_1 [%]	1.72	2.02	1.72	1.74	1.81	1.80	1.83	2.04
ζ_2 [%]	1.31	1.55	1.34	1.32	1.44	1.45	1.69	2.28
ζ_3 [%]	0.69	0.99	0.75	0.73	0.88	0.90	1.00	1.06
ζ_4 [%]	0.59	0.63	0.59	0.60	0.64	0.64	0.64	0.68
ζ_5 [%]	0.42	0.48	0.43	0.46	0.46	0.46	0.51	0.49
ζ_6 [%]	0.32	0.33	0.32	0.33	0.34	0.33	0.34	0.34
MAC_1	1	0.754	0.992	0.977	0.866	0.856	0.950	0.933
MAC_2	1	0.619	0.992	0.992	0.819	0.764	0.514	0.352
MAC_3	1	0.607	0.934	0.941	0.821	0.776	0.626	0.477
MAC_4	1	0.887	0.974	0.968	0.932	0.948	0.947	0.848
MAC_5	1	0.768	0.947	0.710	0.719	0.697	0.676	0.702
MAC_6	1	0.717	0.925	0.911	0.743	0.780	0.685	0.755
MAC_{av}	1	0.725	0.961	0.916	0.817	0.803	0.733	0.678
σ_{max} [MPa]	154	221	157	183	196	190	203	231
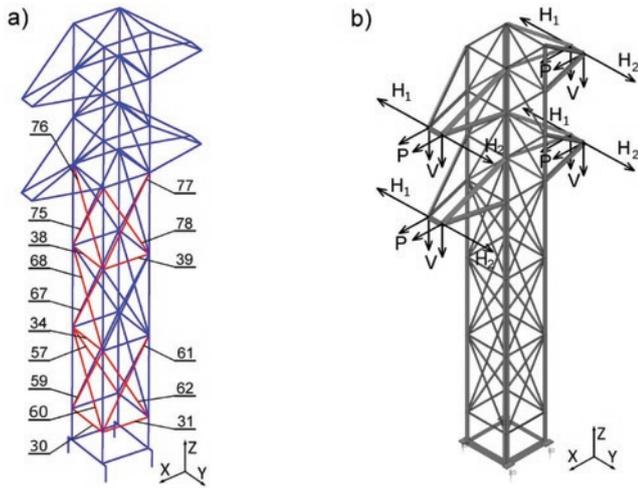
Fig. 9. *Supporting structure (a) numbering of selected elements, (b) forces resulting from loading the structure with wires*

while maximum stress increased by 20% with respect to the nominal condition.

In condition U_7 (Fig. 11c) the same damage as in case U_1 (Fig. 11a) was introduced. Additionally, X-bracing on the neighbouring wall in the same section was removed. This case is extremely unfavourable, and maximum stress increases by 50% with respect to Z_1. Natural frequencies decrease even more than in case U_1, note however that the frequency f_2 for the second mode shape is lower than frequency f_1 for the first mode shape. That is why during the analysis of natural frequencies and/or modal damping ratios it is important to determine the mode shapes for at least a few degrees of freedom in order to identify natural frequencies correctly. The averaged MAC_{av} reaches the lowest values of all analysed cases. However, it should be stressed that MAC_{av} is definitely higher than in case U_1 where the system damage is smaller. The high MAC value results from the fact that damage of the neighbouring bracing restores the tower stem symmetry relative to the plane intersecting points 1, 3, 25, 27 (Fig. 3b), which in turn makes the first mode shape of the damaged structure again similar to the first mode shape of the undamaged structure (Fig. 5a).
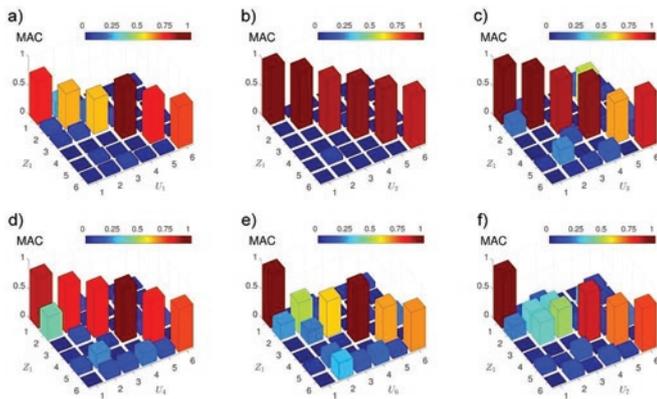
Fig. 10. *Comparison of mode shapes of undamaged structure Z_1 and damaged structure: (a) U_1, (b) U_2, (c) U_3, (d) U_4, (e) U_6, (f) U_7 with the application of MAC criterion*

Cases U_4 and U_5 are characterized by similar damages and involve removal of X-braced panels in segments 3 and 4. The differences between natural frequencies and modal damping ratios for these cases are unnoticeable, the differences can be observed in the 5th and 6th mode shapes, in which legs take the second bending mode. Both damage conditions cause the increase in maximum stress by about

25%, which is a noticeable change, however still about 40 MPa below the material yield stress. Condition U_6 can be treated as an extension of case U_5 – an additional X-bracing damage in the neighbouring wall takes place. Maximum stress exceeds 200 MPa and the structure enters the state of hazard. The averaged MAC_{av} value is lower than in case U_5, but MAC_1 is definitely higher. Similarly to U_1 and U_3, such values of MAC_{av} and MAC_1 result from the fact that the damage restores the tower stem symmetry relative to the plane intersecting points 1, 3, 25, 27 (Fig. 3b) and makes the first mode shape of the damaged structure again similar to the first mode shape of the undamaged structure.

The last analysed case is U_2 (Fig. 11b). The removed elements belong to neighbouring segments, but do not include a simultaneous damage of crossing elements of truss. The damage has a slight impact on the change of modal properties, loss of orthogonality (Fig. 10b) and also on the change of maximum stress in the system. Case U_2 is a good illustration of the problem that it is not the number of damaged elements but their location that poses a threat to the structure stability.
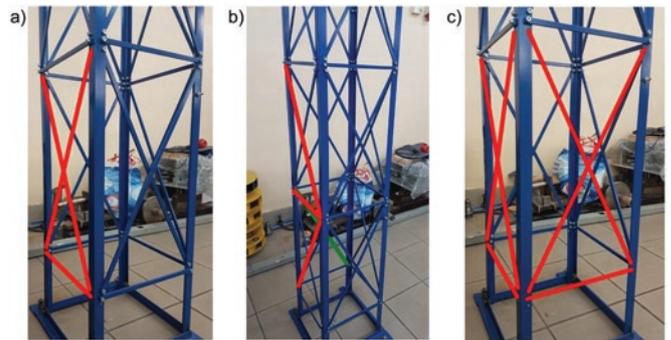
Fig. 11. *Damage condition (a) U_1, (b) U_2, (c) U_7. The removed elements are marked in red and green*

Among the examined natural frequencies, the highest sensitivity to damage is exhibited by f_3, then by f_2 and f_1, the lowest by f_4, then by f_6 and f_5. If the damage involved a removal of X-braced panel, f_3 was reduced by at least 7.5 Hz (22%). In all the analysed cases and for all mode shapes, damping coefficients σ_i did not change noticeably and the increase in the modal damping ratio ζ_i was caused mainly by the change in natural frequencies.

Damage of the whole bracing in one segment of the wall had a significant impact on MAC_1 and MAC_2. For segments 3 and 4 the changes ranged from 0.15 to 0.25, and for segment 2, directly responsible for connection of legs near their restraint, from 0.25 to 0.4. What is important, an additional X-bracing damage in the neighbouring wall (U_6 and U_7) restored the tower stem symmetry relative to the plane that includes the opposite belts, and MAC_1 reached a high value, unlike MAC_2. MAC_3 for the torsional mode shape changed similarly to MAC_2, and for cases in which the maximum stress in the structure exceeded 200 MPa, it was less than 0.63. From among all analysed mode shapes, the fourth mode shape was least sensitive to damage. Damage of middle segments and the truss connecting the legs next to the restraint to the base could be noticed in changes of the fourth and the fifth mode shapes.

For each damage case and applied load, maximum stress in the structure and averaged MAC_{av} for six mode shapes were determined (Fig. 9b). The interrelation of these parameters is shown in Fig. 12. In reality, for a complex-geometry structure this relation is not linear, but it can be approximated using a linear regression model. It should be stressed that the supporting structure load should be selected in a way making it possible to force the work of all bars in the structure while analysed mode shapes should exhibit high sensitivity to damages of all elements.

Damage in the form of local change in structure stiffness affects both the input parameters of the dynamic and static model subject-

ed to the strength analysis. The analysed damage cases indicate that maximum stress in the structure increases as the MAC_{av} decreases. The Pearson correlation coefficient equals $r = -0.963$. The p-value, that is the probability of getting a random variable with at least the same correlation as the observed correlation, when the null hypothesis is fulfilled (H_0: $r = 0$), is equal to $1.18 \cdot 10^{-4}$. These values indicate a very strong negative correlation between quantities and prove that the studies are representative.
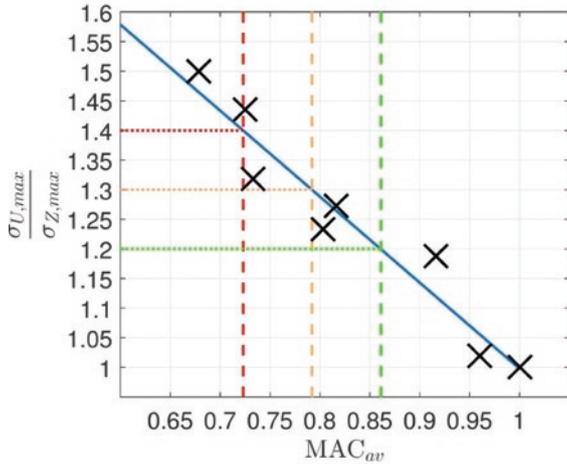
Fig. 12. Relationship between maximum stress in the structure and averaged MAC_{av} value

Four variability ranges of maximum stress in the damaged structure with respect to the undamaged structure were determined, as described by the equation:

$$\delta\sigma_{max} = \frac{\sigma_{U,max} - \sigma_{Z,max}}{\sigma_{Z,max}} \cdot 100\% \qquad (10)$$

and based on the linear regression model, the MAC_{av} variability range was assigned to each of these ranges, to define 4 technical conditions

1. $MAC_{av,d} \geq MAC_{av,g1}$: $\delta\sigma_{max} \leq 20\%$ - safe condition, no significant damage,
2. $MAC_{av,g2} \leq MAC_{av,d} < MAC_{av,g1}$: $20\% < \delta\sigma_{max} \leq 30\%$ - warning condition, slight damage
3. $MAC_{av,g3} \leq MAC_{av,d} < MAC_{av,g2}$: $30\% < \delta\sigma_{max} \leq 40\%$ - dangerous condition, significant damage,
4. $MAC_{av,d} < MAC_{av,g3}$: $\delta\sigma_{max} > 40\%$ - critical condition, damage that directly threatens the stability of the structure

The first condition includes cases where damage has a slight impact on both modal parameters and the change of maximum stress in the system. The $MAC_{av,g1}$ should not exceed 0.9, as this range should also include the errors related to both estimation of the mode shape and the limited number of measuring points. Otherwise, there will be false information indicating more hazard to the structure than in reality. The second warning condition informs about some changes in the structure geometry. The changes are small and are not a hazard for the structure stability, however the modal parameters should be closely monitored. It is recommended to check the structure assigned to condition 2 during the field maintenance. In structures classified

as condition 3, the stress increase significantly in comparison with undamaged structures. Accurate field tests should be performed at the earliest possible occasion and maintenance should be carried out. The fourth case is the critical condition of the structure. If a load occurs that is similar to the simulated load, the maximum stress in the structure will be close to the material yield stress or even will exceed it. The critical condition poses a real threat to the structure stability in the event of loads caused by difficult weather conditions. In the event of a condition 4 message, a technical team should be dispatched immediately to repair the damage. The following limit values were determined in the analysed case: $MAC_{av,g1} = 0.861$, $MAC_{av,g2} = 0.792$, $MAC_{av,g3} = 0.723$. Of course, it should be stressed that MAC_{av} and $\delta\sigma_{max}$ values may be different for various structure types and applied safety criteria.

Verification was performed in two stages. Due to the experiment limitations, the damage shown in Fig. 1 was assumed as one from the damage set from U_1 to U_7, and the experimental analysis was performed instead of the operational modal analysis. In the first stage, the linear regression function was defined based on all damage conditions (Fig. 12). Then it was checked if each condition considered separately is correctly classified based on the MAC_{av} values. In stage two the characteristics defining relationships between the stress change and the MAC_{av} value were determined based on 6 damage conditions, and the seventh condition (not included in the regression analysis) was subject to identification. Seven characteristics were determined in stage two, and each time the data for the damage condition being identified were excluded from calculations.

Table 6 contains identification results for individual damage conditions. All damage cases were correctly identified in the first stage of the method verification. In the second stage only damage no. 6 was identified incorrectly. The error was caused by the fact that the change of the regression input data entails the change in the $MAC_{av,g}$ limit values. It should be emphasized that the maximum absolute difference of any limit value, for all 7 characteristics referred to the characteristics from stage 1 (Fig. 12) did not exceed 0.013 and it was for $MAC_{av,g}$ in case six. In addition, the Fig. 12 indicates that condition U_6 lies at the border of individual technical conditions. It is important that for all determined characteristics the Pearson correlation coefficient was greater than 0.95, indicating a very strong linear relationship.

Considering the obtained results, the proposed identification method of the supporting structure technical condition performs well in the analysed case. Its basic advantage is resistance to measurement, estimation and modelling errors which makes it useful for application under operational conditions.

6. Summary

The supporting structure damage results in the local stiffness decrease, leading to change of both the dynamic response and the stress. Carried out research has proven a strong negative linear correlation between the maximum stress in the system and mode shapes, which makes it possible to identify technical condition of the overhead power line supporting structures. The developed approach is comprehensive and accounts for a number of problems related to the diagnostics of large-size objects of complex geometry.

Truss supporting structures are lightly damped systems, and for the studied case the maximum difference between the damped and undamped natural frequencies amounted to about 0.05%. This means that such a difference is below the modal parameters estimation accu-

Table 6.   Identification of supporting structure technical condition

Identification	U_1	U_2	U_3	U_4	U_5	U_6	U_7
Stage 1	3	1	1	2	2	3	4
Stage 2	3	1	1	2	2	4	4

racy and that, in many cases, simplified models (treating such system as conservative) can be used. Identified numerical model proved to be fine-tuned to the experimental model. Quality criteria were defined for 6 natural frequencies and 6 mode shapes, linking 438 modal parameters. The difference in natural frequencies for five mode shapes was up to 3%, for one - 10% and the MAC for the first five mode shapes was not lower than 0.85.

Under operational conditions the measurement of modal displacements for all degrees of freedom is not possible, so the applied method involved optimum placement of a limited number of sensors in a dynamic system of distributed parameters. By limiting the number of measuring points the experiments were accelerated by 6 to 12 times.

The damping coefficients in analysed cases showed a low sensitivity to damage. The change in modal damping ratios resulted mainly from the change in natural frequency. Therefore, during the identification of damage or technical condition it should be taken into account that the information may be duplicated in some cases.

The basic advantage of the developed algorithm for identification of technical condition of the overhead power line supporting structures is its low sensitivity to measurement errors, which is very important in the context of diagnostics of large-size, complex geometry objects under operational conditions.

References

1. Allemang R J. The Modal Assurance Criterion – Twenty Years of Use and Abuse. Sound and Vibration, 2003; August: 14–21.
2. Bartodziej G, Tomaszewski M. Blackout w rejonie Szczecina. Uwagi i wnioski. Energetyka 2008; nr 10.
3. Chen H P. Application of regularization methods to damage detection in large scale plane frame structures using incomplete noisy modal data. Engineering Structures, 2008; 20(11): 3219–3227, https://doi.org/10.1016/j.engstruct.2008.04.038.
4. Ciesielka W, Szopa K, Gołaś A. The analysis of load of overhead power line due to weather condition and design of smart system of its recognition. Polish Journal of Environmental Studies 2016; 25(5A): 27–36.
5. Dawson B. Vibration condition monitoring techniques for rotating machinery. The Shock and Vibration Digest, 1976; 8: 3, https://doi.org/10.1177/058310247600801203.
6. Dymek D, Jastrzębska E, Kurbiel W. Awarie linii elektroenergetycznych wywołane oblodzeniem. XXVI Konferencja Naukowo Techniczna Awarie Budowlane, Szczecin-Międzyzdroje, 2013; 477–484.
7. Escobar J A, Sosa J J, Gomez R. Structural damage detection using transformation matrix. Computer and Structures 2005; 83: 357–368, https://doi.org/10.1016/j.compstruc.2004.08.013.
8. Esfandiari A, Bakhtiari-Nejad F, Rahai A. Theoretical and experimental structural damage diagnosis method using natural frequencies through an improved sensitivity equation. International Journal of Mechanical Sciences 2013; 70: 79–89, https://doi.org/10.1016/j.ijmecsci.2013.02.006.
9. Ewins D J. Modal testing: Theory and practice. Letchworth, Research Studies Press, 1984.
10. Farrar C R, Doebling S W. An Overview of modal-based damage identification methods. Proceedeings of DAMAS Conference, Sheffield, UK, June, 1997.
11. Gołaś A, Iwaniec M, Szopa K. Hashed data transfer in SHM distributed systems with the use of Power Line Communication technology. Key Engineering Materials 2012; 518: 154–159, https://doi.org/10.4028/www.scientific.net/KEM.518.154.
12. Instytut Meteorologii i gospodarki wodnej. Biuletyn monitoringu klimatu Polski. Warszawa Styczeń 2010.
13. Iwaniec J, Kurowski P. Experimental verification of selected methods sensitivity to damage size and location. Journal of Vibration and Control 2017; 23(7): 1133–1151, https://doi.org/10.1177/1077546315589677.
14. Iwaniec J. Sensitivity analysis of an identification method dedicated to nonlinear systems working under operational loads. Journal of Theoretical and Applied Mechanic, 2011; 49(2): 419–438.
15. Jassim Z, Ali N, Mustapha F, Abdul Jalil N. A review on the vibration analysis for a damage occurrence of a cantilever beam. Engineering Failure Analysis 2013; 31 442–461, https://doi.org/10.1016/j.engfailanal.2013.02.016.
16. Kammer D C. Sensor placement for on-orbit modal identification and correlation of large space structures. Journal of Guidance, Control, and Dynamics 1991; 14(2): 251–259, https://doi.org/10.2514/3.20635.
17. Lam H F, Yin T. Dynamic reduction-based structural damage detection of transmission towers: Practical issues and experimental verification. Engineering Structures 2011. 33: 1459–1478, https://doi.org/10.1016/j.engstruct.2011.01.009.
18. Li D S, Li H N, Fritzen C P. A note on fast computation of effective independence through QR downdating for sensor placement. Mechanical Systems and Signal Processing 2009; 23(4): 1160–1168, https://doi.org/10.1016/j.ymssp.2008.09.007.
19. Maia N M M, Almeida R A B, Urgueira A P V, Sampaio R P C. Damage detection and quantification using transmissibility. Mechanical Systems and Signal Processing 2011; 25: 2475–2483, https://doi.org/10.1016/j.ymssp.2011.04.002.
20. Nobahari M, Seyedpoor M. Structural damage detection using an efficient correlation-based index and a modified genetic algorithm. Mathematical and Computer Modelling 2011; 53 1798–1809, https://doi.org/10.1016/j.mcm.2010.12.058.
21. Paczkowska T, Paczkowski W.: Aspekty budowlane katastrofy energetycznej w rejonie szczecińskim. XXIV Konferencja Naukowo Techniczna Awarie Budowlane, Szczecin-Międzyzdroje 2009; 151–176.
22. Richardson M H, Formenti D L. Parameter estimation from frequency response measurements using rational fraction polynomials, Proceedings, 1st IMAC 1982, Orlando, Fl.
23. Szopa K. Identyfikacja uszkodzeń wielokrotnych konstrukcji mechanicznych z wykorzystaniem modeli zredukowanych. 57. Sympozjon Modelowanie w mechanice, 2018.
24. Szopa K, Iwaniec M, Gołaś A. Low frequency identification of critical states of transmission tower structures. Mechanics and Control 2013; 32(3): 102–109, https://doi.org/10.7494/mech.2013.32.3.102.
25. Urząd Regulacji Energetyki. Podsumowanie dotyczące awarii sieci w grudniu 2009 r. i styczniu 2010 r. na obszarach objętych właściwością poszczególnych operatorów systemów dystrybucyjnych. www.ure.gov.pl, 2010.
26. Worden K, Burrows A P. Optimal sensor placement for fault detection. Engineering Structures 2001; 23(8): 885–901, https://doi.org/10.1016/S0141-0296(00)00118-8.

Krystian SZOPA
AGH University of Science and Technology
Faculty of Mechanical Engineering and Robotics
Department of Power Systems and Environmental Protection Facilities
al. Mickiewicza 30, 30-059 Krakow, Poland

Marek IWANIEC
AGH University of Science and Technology
Faculty of Mechanical Engineering and Robotics
Department of Process Control
al. Mickiewicza 30, 30-059 Krakow, Poland

Joanna IWANIEC
AGH University of Science and Technology
Faculty of Mechanical Engineering and Robotics
Department of Robotics and Mechatronics
al. Mickiewicza 30, 30-059 Krakow, Poland

E-mails: kszopa@agh.edu.pl, iwaniec@agh.edu.pl, jiwaniec@agh.edu.pl